Available online at www.garmian.edu.krd

Passer Journal of Basic and Applied Sciences

Passer 8(Issue 1) (2026) 392-399

Original Article

Sustainable Broadband Antenna Organic Photovoltaics Integration with 100% Insolation

Zhwan Mohammed Rashid*[1,2], Hema Omer Ali[1], Bakhtiar Ali Karim[1,3], Halgurd Nawzad Awl[1]

[1]*Department of Communication, Technical College of Engineering, Sulaimani Polytechnic University, Sulaimani 46001, Iraq.*
[2]*Computer Engineering Department, Tishk International University, Kurdistan Region, Iraq.*
[3]*Faculty of Engineering and Computer Science, Qaiwan International University, Sulaimani, Kurdistan Region, Iraq.*

Received 2 May 2025; revised 24 October 2025;
accepted 05 December 2025; available online 12 January 2026

DOI: 10.24271/PSR.2025.520630.2121

ABSTRACT

This study shows a novel and compact configuration produced by combining an organic solar cell (OSC) with a plus-shaped antenna designed for effective operation in the Ku band. This integrated structure offers an attractive solution for modern satellite communication systems, covering a broad frequency range of 10.6 to 13.7 GHz and providing an efficient 3.1 GHz bandwidth high realized gain of 8.6 dBi with 100% insolation. Building on earlier work that focused on individual performance characteristics, this work highlights its total performance benefits by combining Ku-wide bandwidth, high gain, and full-insolation operating into a single design. The OSC is comprised of aluminum, PH3D, ITO, and Glass materials to ensure an environmentally friendly design. This integration technique offers full solar cell insolation for optimal energy conversion and clearly improves important antenna features, such as a noticeable increase in realized gain by about 2.5 dB and a refined radiation pattern directly attributable to the solar cell. The final design, which offers both performance improvements and environmental concerns, therefore appears as a very practical and environmentally friendly candidate for potential deployments in Ku band satellite technologies.

Keywords: Microstrip Patch Antenna, P3HT: PCBM, Organic Solar Cell, Satellite Communication.

1 Introduction

There has been significant interest in integrating antennas with solar cells over the past two decades. Many engineering applications, including small satellites [1], remote self-powered sensors [2], and wireless monitoring [3] call for sharing the surface area by integrating solar cells and antennas. In isolated regions were setting up a grid electricity transmission is challenging, operating independent communication services for long-term use has become more feasible with a reliable and uninterrupted power supply. Photovoltaic (PV) technology can effectively provide such continuous electricity. The generation of electricity from solar energy might be efficiently achieved in PV devices through the utilization of solar cells designed with different architectures and active materials [4,5]. In addition to minimizing design costs, the power-supply related issues of self-powered applications can be essentially solved by involving solar cells in antenna designs. The microstrip antenna plays a vital role in such systems, providing key advantages including low profile, large broadband gain, and lightweight [6,7]. The first proposal of solar cell-equipped with 2.2 GHz microstrip patch antenna was introduced in 1995 [8] for microsatellite applications. To ensure high performance of the designed antenna, there should be a sufficient distance between the radiating edges of the microstrip patch and the integrated solar cells. Combining patch antennas with photovoltaic cells can help in both saving space and minimizing design costs.

* Corresponding author
E-mail address zhwan.rashid@spu.edu.iq (Instructor).
Peer-reviewed under the responsibility of the University of Garmian.

A literature review revealed that numerous studies have been conducted to equip antennas with solar panels for both satellite and terrestrial applications [9-12]. In this context, several designs and architectures have been suggested to maximize the solar cells' exposure to sunlight, including transparent antenna conductors [13-16] and mesh patch antennas [17-20]. However, it is well known that these designs do not always achieve complete 100% solar exposure, and the incorporation of PV cells is restricted to inorganic solar cells, which are costly and require a high amount of energy during production [21,22]. In recent years, OSCs have attracted considerable interest because of their cost affectedness, lightweight design, flexibility, environmental friendliness, and suitability for ambient solution processing [23,24]. Transparent patch antennas, which offer optical transparency, can be integrated with solar panels on small satellites, helping to tackle the issue of constrained surface area.

For such integration, the antenna must balance high optical transparency to allow solar cells to generate power while maintaining sufficient electrical properties for effective radiation [16].From that perspective, the authors in [15] examined an optimization approach to enhance the radiation efficiency and optical transparency of the antenna. The configuration of an active integrated antenna is applied to meshed patch antennas to boost the power efficiency of the front-end communication subsystem [25,26]. The study in [27] presents an antenna designed with transparent super-wideband coplanar waveguide (CPW) technology, integrated with solar panels for the system of wireless communication requiring mobile power. The achieved antenna's transparency is 63.3%, which is sufficient for effective sunlight utilization.

One of the key problems in integrating solar cells with antennas is ensuring compatibility, preventing the antenna from obstructing the solar cell's functionality while also maintaining the performance of the antenna despite the presence of the solar cell. It is believed that using OSCs with CPW-fed monopole antennas will be particularly beneficial in preventing potential mismatches that could occur when integrating solar cells with antennas. Such a combination could help in maintaining the solar cell's efficiency and the antenna's performance. This results from the fact that organic materials are less prone to attenuation from EM radiation than inorganic materials, making them more resilient in this regard. Additionally, the thickness of the active layer in most OSCs is within the nanometer range [28,29], making it much thinner than the microscale thickness of OSCs [30]. The active layer of the commonly used OSC comprises a mixture of poly(3-hexylthiophene-2,5-diyl) (P3HT) and methanofullerene (PCBM) [31]. This is because these materials exhibit outstanding features, including high optical absorption, strong thermal and electrical characteristics, and chemical stability, positioning them as optimal choices for large-scale OSCs production [32-35]. Besides, various studies [36-39] have integrated the metamaterial (MTM)-based antennas with solar panels to realize self-powered services. From that point of view, the study in [36] presented an MTM-based antenna structure that improves gain by using a solar panel as its substrate. Moreover, the study in [37] proposed an effective design using the solar panel as a reflector for a Vivaldi antenna with a corrugated grating patch based on MTM. In [38], a plasmonic MTM antenna array was printed on a flexible solar panel for modern applications. Lastly, the authors in [39] suggested a new MTM-based antenna design in which the ground plane of the antenna was connected to the designed solar panel.

This work presents a new configuration of an integrated OSC. The antenna is composed of a coplanar waveguide (CPW) feed structure with a plus-shaped radiating patch. An OSC is designed and placed at the back of the antenna. The OSC consists of four materials: aluminum, PH3D, ITO, and Glass. The OSC has 100% insolation and is not only compatible with the designed antenna but also improves antenna performance, such as gain and radiation pattern. The proposed antenna solar cell integration operated at the KU band applications, especially the required range of satellite communications.

The rest of the paper is organized as follows. In Section 2, the methodology of the designed antenna is revealed. Section 3 presents and comprehensively discusses the achieved results. Section 4 concludes the primary results of the paper.

2 Methodology

2.1 Design structure

The suggested antenna solar cell integration is presented in Figure 1. The antenna compromises of a plus-shaped radiated patch at the top layer, Figure 1(a), with a CPW structure at the bottom side, Figure 1(b). The substrate material is RD druid 5880 with 2.2 relative permittivity, which is sandwiched between the radiating patch and the feeding structure. A conducting layer at the antenna's top and bottom sides is made of copper material with 0.035 mm thickness and conductivity of 5.96 ×10^7 S/m. The antenna is integrated with an OSC on the back side of the antenna with a 25 mm gap thickness. The existing gap provides multi-mode operation besides the CPW feed and guarantees broadband operation of the antenna over the KU band frequency range. The proposed solution was specifically selected to enable 100% OSC insolation, enhancing the antenna's performance. A 3x4 array of solar cells connected in series and parallel produces an average open circuit voltage of approximately 1.2 V and a short-circuit current density of around Jsc = 20 mA/cm^2. The CST studio suite is used as a numerical solution for the design and simulation of the structure, and a genetic algorithm is applied to optimize the proposed design. Table 1 presents the optimal dimension of the designed structure.

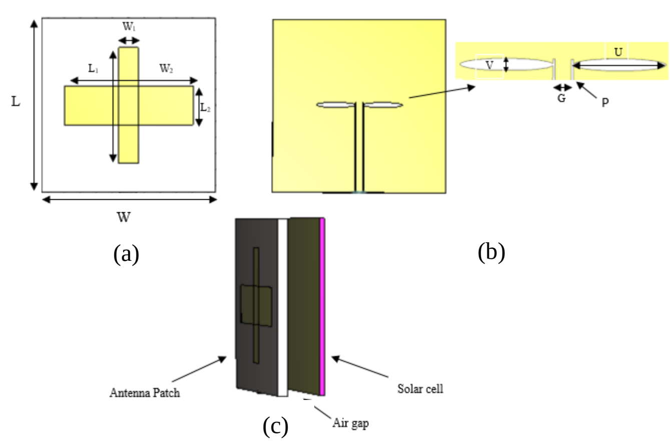

Figure 1: The suggested antenna design, (a) front view, (b) back view, (c) antenna integrated solar cell.

Table 1: The optimal design specifications of the proposed Broadband antenna.

Parameters	Value (mm)
W	54
L	54
W_1	2
L_1	36

W_2	20
L_2	10
U	6.1
V	0.8
G	2.1
P	0.3

2.2 Structure of the OSC

In this integrated design, the organic solar cell (OSC) is positioned atop a glass substrate, which was selected for its cost-effectiveness, mechanical stability, and appropriate dielectric characteristics at the working frequency. To guarantee strong adherence for ensuing layers, the glass substrate utilized in this investigation is 5 mm thick.

A thin 20 nm-thick indium tin oxide (ITO) electrode is the first functional layer to be placed onto the glass. By acting as the front electrode in the OSC, ITO—a popular transparent conductive oxide—allows incident light to reach the active layer. As shown in Table 2, its high bulk conductivity of 10^6 S/m is essential for effective lateral charge transport and collection. At the interface with the P3HT: PCBM layer, the ITO's work function makes charge injection and extraction easier. For the best solar cell performance, the 20 nm thickness strikes a balance between obtaining enough conductivity and preserving enough transparency. Sputtering is frequently used to deposit ITO layers because it provides accurate control over thickness.

The 100 nm-thick P3HT: PCBM organic active layer forms the OSC's core. This combination of [6,6]-phenyl-C61-butyric acid methyl ester (PCBM) and Poly(3-hexylthiophene) (P3HT) is a well-known photoactive material system in OSCs because of its effective charge separation at the donor-acceptor heterojunction and wide spectrum absorption. [Excitons, or electron-hole pairs, are produced in the P3HT when photons are absorbed]. They then diffuse to the P3HT/PCBM interface, where their ionization potentials and electron affinities differ, effectively separating them. The electromagnetic interaction between this active layer and the antenna construction is greatly influenced by its electrical characteristics, which include a relative permittivity of 3.920 and a bulk conductivity of 0.300 S/m (Table 2). A trade-off between increasing light absorption in the active layer and guaranteeing effective exciton diffusion to the charge separation interface led to the selection of the 100 nm thickness.

Lastly, the P3HT: PCBM layer is covered with an aluminum electrode that is 200 nm thick. Because of its high electrical conductivity (10^6 S/m, Table 2), appropriate work function for effective electron collection from the P3HT: PCBM layer, good adhesion to the organic active layer that ensures effective charge transfer, and relative affordability and ease of deposition, aluminum was chosen as the back electrode. Electrons that have passed through the active layer can be collected more easily thanks to this layer. Good electrical contact throughout the active area and low series resistance are guaranteed by the 200 nm thickness. Usually, heat evaporation is used to deposit aluminum electrodes.

This multilayer OSC structure is placed into the backside of the plus-shaped antenna design, as shown in Figure 2. In addition to harvesting solar energy, this integration has a major impact on the antenna's electromagnetic performance, as will be covered in Section 3.

Table 2: The OSC electrical and magnetic parameters that are used in the recommended antenna design.

Parameters	P3HT: PCBM	ITO
Relative permittivity	3.920	3.6150
Relative permeability	1.010	1.0001
Bulk conductivity (S/m)	0.300	10^6

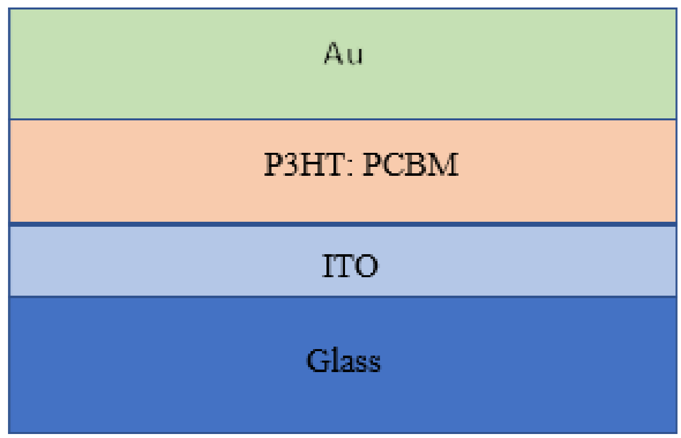

Figure 2: Illustration of the proposed OSC layers.

Using solution-based methods like spin-coating or roll-to-roll printing, organic solar cells (OSCs) can be produced at temperatures below 150 °C. This significantly decreases energy consumption compared to crystalline silicon or CIGS/III–V technologies, which require processing temperatures exceeding 500 °C [40,41] In addition to reducing production costs and carbon emissions, this low-temperature fabrication enables the deposition of OSCs on flexible substrates, such as PET or PEN, for applications that require flexibility and lightweight properties [42]. OSCs are quit environmentally friendly as they don't contain harmful heavy metals like Cd or Pb and process solutions under ambient conditions, which lowers environmental and occupational risks [43]. Additionally, life-cycle analyses show that OSCs have a significantly shorter energy payback time (EPBT)—between roughly 0.14 and 1.1 years—and a lower cumulative energy demand (CED) than crystalline silicon modules, which have an EPBT of 1.5 to 2.5 years [44]. Furthermore, their materials—which include organic semiconductors, glass, and aluminum—offer great recyclability, reducing waste and promoting circular sustainability [44]. All things considered, OSCs offer a versatile, low-energy, and environmentally friendly photovoltaic platform that supports international initiatives for sustainable solar energy solutions [40,44].

3 Results and Discussions

3.1 The impact of the OSC on the performance of the designed antenna

At the first stage, the advised antenna was designed, simulated, and optimized separately. In the second stage, the influence of the OSC on the designed antenna performance was investigated. For this purpose, the reflection coefficient and realized gain of the antenna with and without a solar cell are presented in Figures 3 and 4, respectively. It can be seen that the proposed antenna operated over the frequency range of (10.6- 13.7) GHz, with 3.1 GHz over the KU band and three resonance frequencies of 11.2 GHz, 12.2 GHz, and 13.82 GHz. The incorporation of the solar cell leads to a minor decrease in return loss magnitude and a slight frequency shift; nevertheless, the suggested system continues to operate within the same frequency band and remains entirely appropriate for its intended purpose. Following the frequency designated by the International Telecommunication Union (ITU), this is regarded as an interesting frequency for satellite applications.

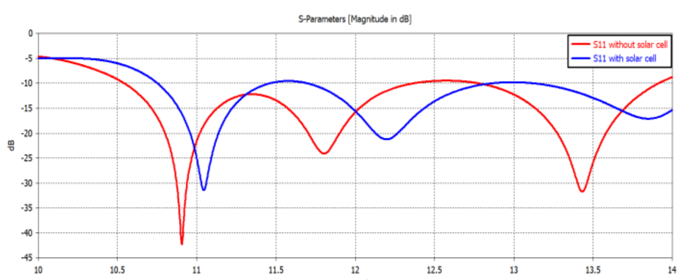

Figure 3: Simulated S_{11} results of the microstrip antenna with and without the integrated OSC.

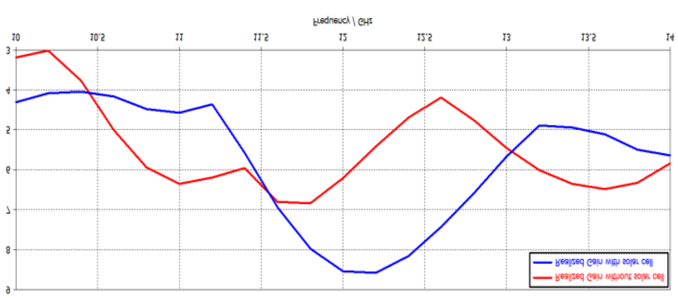

Figure 4: Realized gain of the designed microstrip antenna in the presence and absence of the OSC.

The integration of the solar cell with the designed antenna provides the advantage of a gain increment of about 2.5 dB center frequency of 12 GHz, which is very important for the satellite application at the range of 11.7 -12.33 GHz. The obtained realized gain of the integrated antenna solar cell fluctuates with a maximum gain of 8.6 dB at 12.1 GHz. The enhancement in antenna gain with solar-cell integration mostly results from increased impedance matching, constructive field coupling, and improved directivity attributable to the electromagnetic and dielectric characteristics of the solar cell.

3.2 Effect of the Gap thickness between antenna and solar cell thickness on S-parameters and realized gain

Here, the influence of the gap thickness between the proposed antenna and the OSC on the reflection coefficient and realized gain was investigated. For this purpose, the gap thickness was changed from 5 mm to 30 mm, and the obtained results are presented in Figures 5 and 6. It can be noted that the gap variation does not have much impact on the operating frequency range, as the antenna relatively works at the same frequency range as the internet. However, when the gap is not enough, increased reactive coupling occurs, resulting in impedance mismatching and increasing reflection losses. Conversely, when the gap is very wide, the advantageous electromagnetic contact between the antenna and the solar cell diminishes, hence impairing overall performance. A separation of 25 mm achieves the greatest equilibrium between coupling and field interaction, yielding the most profound return loss, enhanced impedance matching, and maximum radiation efficiency.

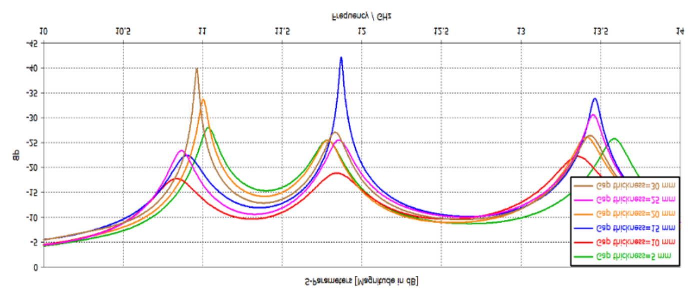

Figure 5: The impact of gap thickness on the reflection coefficient of the designed antenna solar cell structure.

As illustrated in Figure 6, the thickness of the gap between the solar cell and the antenna significantly influences the antenna's gain performance. The realized gain of the antenna increased with the gap increment and gap thickness increment, except for the 30 mm value. Therefore, the gap thickness of the proposed design was kept at 25 mm for the best gain increment of the structure, which roughly aligns with a quarter-wavelength separation at the operational frequency, resulting in constructive interference, less loss, and improved realized gain.

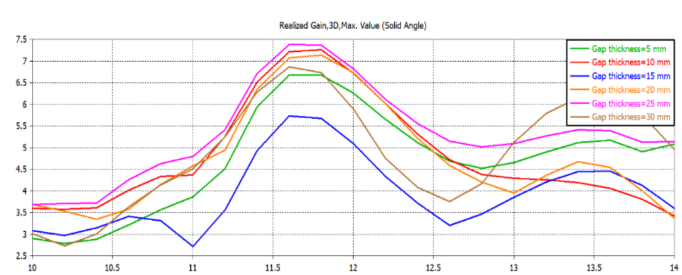

Figure 6: The influence of gap thickness on the realized gain of the designed antenna solar cell structure.

3.3. The impact of patch size variation on S-Parameters and gain

As presented in Figure 1 (a), the radiating patch of the proposed antenna consists of vertical and horizontal conducting strip lines making a plus shape. The size of these conducting strips influences the performance of the antenna significantly. For this purpose, the width of the vertical strip (W_1) and length of the horizontal strip (L_2) have been changing; the corresponding reflection coefficient and realized gain results are shown in Figures 7-10. It can be seen from Figure 7 that the realized gain increases with vertical strip width increment. However, the skinny and thick vertical strip width increases the mismatch of the antenna. Changing the length of the radiating strip in the plus-shaped patch antenna significantly affects both the resonance frequency and the radiation gain. Extending the strip length reduces the resonance frequency and initially enhances radiation owing to a wider effective aperture. Nevertheless, beyond an ideal threshold (about L2 = 14 mm), the antenna encounters a mismatch and diminished efficiency. Therefore, meticulous adjustment of the strip length is crucial to attain the optimal equilibrium among bandwidth, impedance matching, and gain performance.

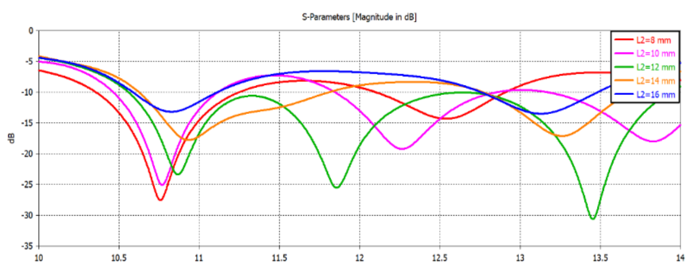

Figure 7: The impact of horizontal strip length (L_2) variation on the simulated reflection coefficient response.

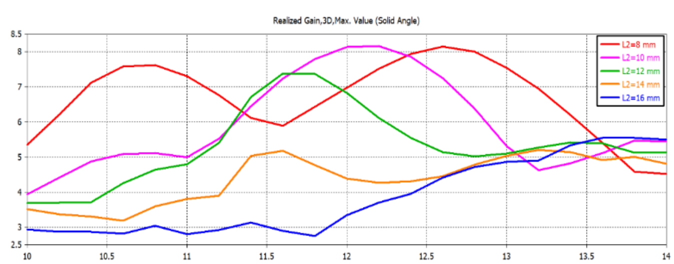

Figure 8: The illustration of how the variation of horizontal strip length (L_2) influences the realized gain.

Figures 9 and 10 show that changing the vertical strip width (W_1) greatly affects the S_{11} and realized gain response. Altering the vertical strip width (W_1) significantly impacts the impedance matching and radiation gain of the plus-shaped antenna. Initially, increasing the width enhances matching and gain due to an expanded radiating area and improved current flow. However, beyond an ideal threshold (W_1 = 6 mm), excessive capacitive coupling and current distortion impair performance. Therefore, a moderate width of approximately 6 mm provides the optimal balance of bandwidth, impedance matching, and gain efficiency, guaranteeing stable performance across the Ku-band.

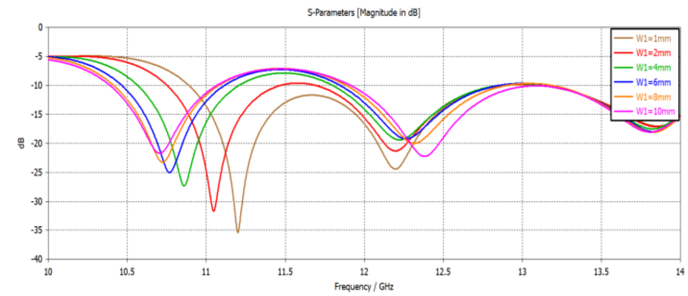

Figure 9: The illustration of how the variation of vertical strip width (W_1) influences the reflection coefficient response.

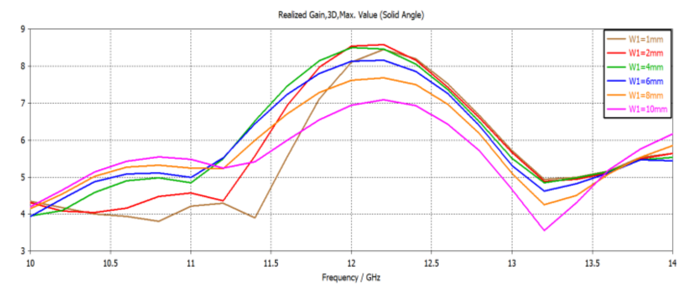

Figure 10: The illustration of how the variation of vertical strip width (W_1) influences the realized gain.

3.4 Radiation pattern

Figure 11 illustrates the directional radiation pattern of the proposed antenna integrated with the solar cell. At 12 GHz center frequency, a highly directional radiation pattern with a narrow half-power beamwidth is obtained at the E-plane. It is worth mentioning that the existence of the solar cell and gap thickness variation has a great impact on improving the radiation pattern. The higher thickness improves the radiation shape and, on the other hand, reduces realized gain. Therefore, the distance can be modified according to the requirement.

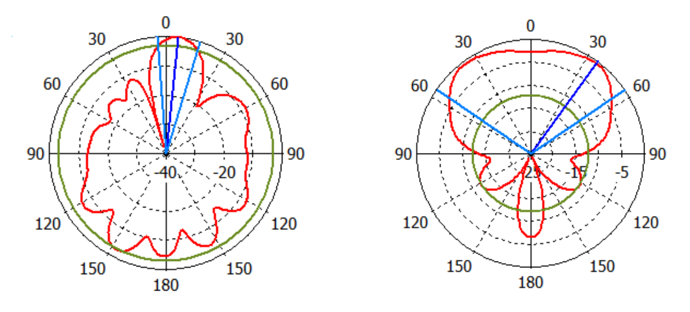

E- H-

Figure 11: Simulation results of the radiation patterns for the antenna–solar cell configuration at 12 GHz.

According to the comparison presented in Table 3, the suggested antenna design exhibits a notable bandwidth advantage, reaching

3.1 GHz throughout the Ku band (10.6 - 13.7 GHz). This increased bandwidth provides more flexibility than many of the referenced designs, which have smaller operational ranges, and is essential for addressing the rising data transmission rates and channel allocations required by modern satellite communication systems. The real innovation is in the synergistic integration of the organic solar cell (OSC), even though the competitive gain of 8.6 dB satisfies the gain numbers of references.

The OSC's strategic positioning and design allow for 100% solar cell insolation, which distinguishes this work from most of the antennas under comparison. As demonstrated by the previously discussed improved gain and radiation characteristics, this full insolation not only suggests significant energy harvesting potential, enabling self-powered operation or additional power for related electronics, but it also enhances the antenna's electromagnetic performance. In contrast to traditional antenna designs, which frequently overlook energy harvesting or use distinct, possibly less effective solar cell configurations, our integrated approach provides a small and multipurpose solution. This significant and competitive bandwidth, along with the unique benefit of integrated energy harvesting via a fully insolated organic solar cell, makes the suggested antenna-solar cell integration an exceptionally desirable and innovative choice for future Ku band satellite applications that deal with communication efficiency and power autonomy.

Table 3: Evaluation of the proposed antenna in relation to the previously published studies.

Ref.	Bandwidth (GHz)	Gian (dB)	Application	Insolation %
[45]	0.33	10.85	5G communication	28.07
[46]	0.1	2.79	Wi-Fi	99
[11]	1.16	8.8	CubeSat	79
[47]	0.175 0.4	5.7 6.93	IoT over Satellite	Not 100
[48]	10	5.9	Satellite	100
[49]	4.1	6.05	Satellite	87
[50]	5.07	4.5	Energy Harvesting	100
Current work	3.1	8.6	Satellite	100

4 Conclusions

This study presents the design and optimization of an integrated organic solar cell (OSC) antenna system for Ku-band satellite communication applications under conditions of complete insolation. The proposed configuration integrates a plus-shaped radiating patch antenna with a multilayer organic solar cell, facilitating concurrent energy harvesting and high-performance wireless functionality without mutual degradation. Thorough parametric analyses were performed to examine the influence of critical design variables—such as the solar cell integration gap, patch dimensions, and strip geometry—on the antenna's impedance and radiation properties. The proposed antenna solar cell integration operated over a frequency range of 10.6–13.7 GHz to be used for satellite Ku band applications. The OSC is comprised of four materials, including aluminum, PH3D, ITO, and Glass materials to guarantee an environmentally sustainable design. Full OSC insolation is attained, improving antenna performance through this integration. The design specifically demonstrates 3.1 GHz, which is within an ITU downlink, the substantially improved gain of 8.1dB, and a significantly enhanced radiation pattern with the existence of the OSC. Directional radiation properties characterize the antenna, confirming its capability for directional telecommunication applications, such as satellite.

Table of Symbols

Symbol	Definition
Jsc	Short-current density mA/cm^2
S_{11}	reflection coefficient (dB)
W, L, W_1, L_1, W_2, L_2, U, V, G, P	Parameters of Broadband antenna (mm)

Funding

This research received no external funding.

Acknowledgements

This work was conducted independently and has not received any financial or institutional support from any organization.

Authors contribution

The conceptualization of the study was carried out by Zhwan Mohammed Rashid and Halgurd Nawzad Awl, while the methodology was developed by Zhwan Mohammed Rashid and Hema Omer Ali. Software implementation was handled by Halgurd Nawzad Awl, and validation was performed by Hema Omer Ali and Bakhtiar Ali Karim. Halgurd Nawzad Awl also conducted the formal analysis, with investigation efforts contributed by both Bakhtiar Ali Karim and Hema Omer Ali. The necessary resources were provided by Bakhtiar Ali Karim and Zhwan Mohammed Rashid. Data curation was managed by Halgurd Nawzad Awl. The initial version of the manuscript was prepared by Bakhtiar Ali Karim and Zhwan Mohammed Rashid, while review and editing were undertaken by Bakhtiar Ali Karim and Halgurd Nawzad Awl. Supervision was the responsibility of Halgurd Nawzad Awl, and project administration was led by Zhwan Mohammed Rashid.

Conflict of interest

The authors declare no conflicts of interest

References

[1] Vaccaro, S., Pereira, C., Mosig, J. R. & De Maagt, P. In-flight experiment for combined planar antennas and solar cells (SOLANT). *IET Microw. Antennas Propag.* **3**, 1279–1287, doi:10.1049/iet-map.2008.0410 (2009).

[2] Wu, T., Li, R. & Tentzeris, M. M. A scalable solar antenna for autonomous integrated wireless sensor nodes. *IEEE Antennas Wirel. Propag. Lett.* **10**, 510–513, doi:10.1109/LAWP.2011.2152357 (2011).

[3] O'Conchubhair, O., McEvoy, P. & Ammann, M. J. Integration of antenna array with multicrystalline silicon solar cell. *IEEE Antennas Wirel. Propag. Lett.* **14**, 1231–1234, doi:10.1109/LAWP.2015.2399652 (2015).

[4] Sampaio, P. G. V. & González, M. O. A. Photovoltaic solar energy: Conceptual framework. *Renew. Sustain. Energy Rev.* **74**, 590–601, doi:10.1016/j.rser.2017.02.081 (2017).

[5] Muhammad, F. F. & Sulaiman, K. Photovoltaic performance of organic solar cells based on DH6T/PCBM thin film active layers. *Thin Solid Films* **519**, 5230–5233, doi:10.1016/j.tsf.2011.01.165 (2011).

[6] Tonui, P., Oseni, S. O., Sharma, G., Yan, Q. & Mola, G. T. Perovskites photovoltaic solar cells: An overview of current status. *Renew. Sustain. Energy Rev.* **91**, 1025–1044, doi:10.1016/j.rser.2018.04.069 (2018).

[7] Maharaja, M. & Kalaiselvan, C. Integration of antenna and solar cell for satellite and terrestrial communication. *Int. J. Sci. Res. Publ.* **3**, 1–5 (2013).

[8] Tanaka, M., Suzuki, R., Suzuki, Y. & Araki, K. *IEEE*, 786–789 (year not specified).

[9] O'Conchubhair, O., Narbudowicz, A., McEvoy, P. & Ammann, M. J. Circularly polarised solar antenna for airborne communication nodes. *Electron. Lett.* **51**, 667–669, doi:10.1049/el.2015.0201 (2015).

[10] Al-Adhami, A., Al-Adhami, Y. & Elwi, T. A. A 3D antenna array based solar cell integration for modern MIMO systems. *Infocommun. J.* **15**, doi:10.36244/ICJ.2023.4.2 (2023).

[11] Wang, H., Park, Y. B. & Park, I. Low-profile wideband solar-cell-integrated circularly polarized CubeSat antenna for the Internet of Space Things. *IEEE Access* **10**, 61451–61462, doi:10.1109/ACCESS.2022.3182108 (2022).

[12] Mahmoud, M. N. & Baktur, R. Integrated solar panel slot antennas certified for CubeSat missions. *IEEE Open J. Antennas Propag.*, doi:10.1109/OJAP.2024.3385288 (2024).

[13] Roo-Ons, M. J., Shynu, S. V., Ammann, M. J., McCormack, S. J. & Norton, B. Transparent patch antenna on a-Si thin-film glass solar module. *Electron. Lett.* **47**, 85–86, doi:10.1049/el.2010.7397 (2011).

[14] Moharram, M. A. & Kishk, A. A. Optically transparent reflectarray antenna design integrated with solar cells. *IEEE Trans. Antennas Propag.* **64**, 1700–1712, doi:10.1109/TAP.2016.2539379 (2016).

[15] Yasin, T. Transparent antennas for solar cell integration. *Utah State University* (2013).

[16] Emon, E. I., Islam, A. M., Bashar, M. S. & Ahmed, A. Design, fabrication, and performance analysis of a silicon solar cell integrated transparent antenna for wireless communications. *Eng. Sci. Technol. Int. J.* **61**, 101915, doi:10.1016/j.jestch.2024.101915 (2025).

[17] Turpin, T. W. & Baktur, R. Meshed patch antennas integrated on solar cells. *IEEE Antennas Wirel. Propag. Lett.* **8**, 693–696, doi:10.1109/LAWP.2009.2025522 (2009).

[18] Sheikh, S. Circularly polarized meshed patch antenna. *IEEE Antennas Wirel. Propag. Lett.* **15**, 352–355, doi:10.1109/LAWP.2015.2445836 (2015).

[19] Silva, Z. J., Hunter, C. P., Valenta, C. R. & Durgin, G. D. 843–844 (IEEE).

[20] Sheikh, S. & Shokooh-Saremi, M. 198–201 (IEEE).

[21] Yurduseven, O. & Smith, D. Solar cell stacked dual-polarised patch antenna for 5.8 GHz band WiMAX network. *Electron. Lett.* **49**, 1514–1515, doi:10.1049/el.2013.2451 (2013).

[22] O'Conchubhair, O., Yang, K., McEvoy, P. & Ammann, M. J. Amorphous silicon solar Vivaldi antenna. *IEEE Antennas Wirel. Propag. Lett.* **15**, 893–896, doi:10.1109/LAWP.2015.2479189 (2015).

[23] Deng, B. *et al.* The art and science of translucent color organic solar cells. *Nat. Commun.* **16**, 597, doi:10.1038/s41467-025-55924-9 (2025).

[24] Zhai, Y., Chang, Y., Tang, A. & Lu, K. A review of photostability in organic solar cells: from mechanisms to improvement strategies. *J. Mater. Chem. A* (2025).

[25] Ali, S. H., Abdulkarim, Y. I. & Mohammed, H. O. Flexible wearable antenna incorporating metasurface for WBAN applications. *Passer J. Basic Appl. Sci.* **6**, 8–15, doi:10.24271/psr.2023.411415.1369 (2024).

[26] Saeed, M. H. R. Design and simulation of rectangular microstrip patch antennas (45 GHz and 60 GHz) for V-band applications. *Passer J. Basic Appl. Sci.* **4**, 100–104, doi:10.24271/psr.2022.333252.1124 (2022).

[27] Rohaninezhad, M., Jalali Asadabadi, M., Ghobadi, C. & Nourinia, J. Design and fabrication of a super-wideband transparent antenna implanted on a solar cell substrate. *Sci. Rep.* **13**, 9977, doi:10.1038/s41598-023-37073-5 (2023).

[28] Dennler, G., Scharber, M. C. & Brabec, C. J. Polymer-fullerene bulk-heterojunction solar cells. *Adv. Mater.* **21**, 1323–1338, doi:10.1016/S1369-7021(11)70210-3 (2009).

[29] Etxebarria, I., Ajuria, J. & Pacios, R. Solution-processable polymeric solar cells: A review on materials, strategies and cell architectures. *Org. Electron.* **19**, 34–60, doi:10.1016/j.orgel.2015.01.014 (2015).

[30] Parola, S., Julián-López, B., Carlos, L. D. & Sanchez, C. Optical properties of hybrid organic-inorganic materials and their applications. *Adv. Funct. Mater.* **26**, 6506–6544, doi:10.1002/adfm.201602730 (2016).

[31] Reyes-Reyes, M., Kim, K. & Carroll, D. L. High-efficiency photovoltaic devices based on annealed P3HT:PCBM blends. *Appl. Phys. Lett.* **87,** doi:10.1063/1.2006986 (2005).

[32] Moerland, R. J. & Hoogenboom, J. P. (2016).

[33] Stelling, C. *et al.* Plasmonic nanomeshes as transparent electrodes in organic solar cells. *Sci. Rep.* **7**, 42530, doi:10.1038/srep42530 (2017).

[34] Ahmad, Z., Awais, M., Najeeb, M. A., Shakoor, R. A. & Touati, F. P3HT, PBLG, and PMMA as energy harvesting materials. *Smart Polym. Nanocompos.*, 95–118, doi:10.1007/978-3-319-50424-7_4 (2017).

[35] Moerland, R. J. & Hoogenboom, J. P. Subnanometer optical distance ruler based on fluorescence quenching. *Optica* **3**, 112–117, doi:10.1364/OPTICA.3.000112 (2016).

[36] Jawad, M. A. *et al.* Dielectric properties of mortar for wireless networks. *Prog. Electromagn. Res. Lett.* **89**, 91–97, doi:10.2528/PIERL19090912 (2020).

[37] Mishra, P. & Pattnaik, S. S. Metamaterial-loaded fractal interdigital capacitor antenna. *Prog. Electromagn. Res. M* **70**, 127–134, doi:10.2528/PIERM18032801 (2018).

[38] Alnaiemy, Y., Elwi, T. A. & Nagy, L. Mutual coupling reduction using EBG structures. *Period. Polytech. Electr. Eng. Comput. Sci.* **63**, 332–342, doi:10.1029/2021RS007392 (2019).

[39] Elwi, T. A. & Abdulqader, S. G. Investigation of SOLANT–rectenna-based flexible Hilbert metamaterials. *IET Nanodielectr.* **3**, 88–93, doi:10.1049/iet-nde.2020.0013 (2020).

[40] 3GPP 38.901. *Study on channel model for frequencies from 0.5 to 100 GHz.* Release 17 (2022).

[41] Solak, E. K. & Irmak, E. Advances in organic photovoltaic cells. *RSC Adv.* **13**, 12244–12269, doi:10.1039/D3RA01454A (2023).

[42] Carrillo-Sendejas, J. C. & Maldonado, J.-L. Progress in organic solar cells. *APL Energy* **3**, doi:10.1063/5.0267160 (2025).

[43] Sun, S. *et al.* Origin of high efficiency in low-temperature hybrid perovskite solar cells. *Energy Environ. Sci.* **7**, 399–407, doi:10.1039/C3EE43161D (2014).

[44] Anctil, A., Lee, E. & Lunt, R. R. Energy and cost benefit of transparent solar cells for buildings. *Appl. Energy* **261**, 114429, doi:10.1016/j.apenergy.2019.114429 (2020).

[45] Luo, Y., Lai, J., Yan, N., An, W. & Ma, K. Dual-mode aperture-coupled patch antenna integrated with solar cells. *IEEE Antennas Wirel. Propag. Lett.* **20**, 1468–1472, doi:10.1109/LAWP.2021.3087500 (2021).

[46] Ali, A., Wang, H., Lee, J., Ahn, Y. H. & Park, I. Ultra-low profile solar-cell integrated antenna. *Sci. Rep.* **11**, 20918, doi:10.21203/rs.3.rs-795538/v1 (2021).

[47] Baccouch, C., Bahhar, C., Sakli, H. & Aguili, T. Adaptive Ku-band solar rectenna for IoT-over-satellite. *Wirel. Commun. Mob. Comput.* **2021**, 9934025, doi:10.1155/2021/9934025 (2021).

[48] Abdulkarim, Y. I. *et al.* Broadband CPW-fed antenna with organic solar cells under 100% insolation. *Materials* **13**, 142, doi:10.3390/ma13010142 (2019).

[49] Nashad, F. *et al.* Ku-band suspended meshed patch antenna integrated with solar cells. *Prog. Electromagn. Res. C* **83**, 245–254, doi:10.2528/PIERC18020608 (2018).

[50] Cheng, F., Cheng, B.-Y., Li, H.-P. & Ni, W. Broadband omnidirectional rectenna with solar-cell integration. *Energies* **18**, 5098, doi:10.3390/en18195098 (2025).